

A SIGNATURE OF CHEMICAL SEPARATION IN THE COOLING CURVES OF TRANSIENTLY ACCRETING NEUTRON STARS

ZACH MEDIN¹ AND ANDREW CUMMING²¹Los Alamos National Laboratory, Los Alamos, NM 87545, USA; zmedin@lanl.gov and²Department of Physics, McGill University, 3600 rue University, Montreal, QC, H3A 2T8, Canada; cumming@physics.mcgill.ca
Draft version November 24, 2018

ABSTRACT

We show that convection driven by chemical separation can significantly affect the cooling curves of accreting neutron stars after they go into quiescence. We calculate the thermal relaxation of the neutron star ocean and crust including the thermal and compositional fluxes due to convection. After the inward propagating cooling wave reaches the base of the neutron star ocean, the ocean begins to freeze, driving chemical separation. The resulting convection transports heat inward, giving much faster cooling of the surface layers than found assuming the ocean cools passively. The light curves including convection show a rapid drop in temperature weeks after outburst. Identifying this signature in observed cooling curves would constrain the temperature and composition of the ocean as well as offer a real time probe of the freezing of a classical multicomponent plasma.

Subject headings: dense matter — stars: neutron — X-rays: binaries — X-rays: individual

1. INTRODUCTION

The observation of surface cooling of accreting neutron stars on timescales of days to years after they go into quiescence has opened up a new window on the physics of neutron star crusts. Six neutron stars in low mass X-ray binaries have now been observed to cool after extended accretion outbursts that were long enough to heat the crust significantly out of thermal equilibrium with the core (Cackett et al. 2010, 2013; Fridriksson et al. 2011; Degenaar et al. 2011, 2013a,b). The subsequent thermal relaxation of the crust depends on its physical properties such as its thickness, thermal conductivity, and heat capacity, with deeper regions being probed at successively later times in the cooling curve (Eichler & Cheng 1989; Brown & Cumming 2009, hereafter BC09). Shternin et al. (2007) and BC09 showed that the observed cooling curves of KS 1731–260 and MXB 1659–29 imply that the inner crust has a thermal conductivity corresponding to an impurity parameter of order unity. Page & Reddy (2013) find that the cooling curve of XTE J1701–462 is compatible with similar crust microphysics to KS 1731–260 and MXB 1659–29.

Chemical separation occurs when, as a material freezes, the equilibrium compositions of the liquid and solid phases are different. This important process can drive sedimentation or mixing in white dwarf (Althaus et al. 2012) and giant planet (e.g., Wilson & Militzer 2010) interiors, and Earth’s core (Hirose et al. 2013). Horowitz et al. (2007) carried out molecular dynamics simulations of the freezing of the multicomponent plasma expected in the outer layers of accreting neutron stars, and found chemical separation occurred, with lighter nuclear species being preferentially retained in the liquid phase. In a previous paper (Medin & Cumming 2011, hereafter MC11) we considered the effect of chemical separation while accretion is ongoing. In that case, as matter is driven to higher pressure and crosses the freezing depth, the light elements released into the neutron star ocean will drive convec-

tion, mixing them throughout the ocean and raising the light element fraction. At the same time, because the convection is driven by composition gradients in an otherwise thermally stable layer, the convective heat flux is inward, potentially heating the layers deep in the ocean.

In this paper, we consider the cooling of the outer layers of the star in quiescence, during which the liquid layers freeze into a solid and chemical separation occurs, enriching the ocean further in light elements. We show that the resulting compositionally driven convection can significantly modify the expected cooling curves of accreting transients. We first discuss the expected size of the compositionally driven heat flux and show that it is easily comparable to the cooling flux in the ocean (§2). We then present simulations of ocean cooling including heat transport by convection, showing that the light curve is significantly modified (§3). We conclude with a discussion of the theoretical uncertainties and implications for observed sources (§4).

2. CHEMICAL SEPARATION AND THE COMPOSITIONALLY DRIVEN HEAT FLUX

The outermost layers of an accreting neutron star form a gaseous atmosphere and liquid ocean (Bildsten & Cutler 1995), in regions where the Coulomb coupling parameter $\Gamma \equiv \langle Z^{5/3} \rangle e^2 / a k_B T < 175$ (Potekhin & Chabrier 2000), where $\langle Z^{5/3} \rangle$ is the number average over the mixture of nuclei with charge Z_i , a is the internuclear spacing, and T is the temperature. A useful measure of the depth is the column depth y , related to the pressure by $P = gy$ where g is the gravity. The base of the ocean lies at

$$y_{b,14} = 1.8 \left(\frac{T_{b,8}}{3} \right)^4 \left(\frac{\langle Z_b^{5/3} \rangle}{100} \right)^{-4} \left(\frac{g_{14}}{2} \right)^{-1}, \quad (1)$$

where $y_{14} = y/10^{14} \text{ g cm}^{-2}$, $T_8 = T/10^8 \text{ K}$, $g_{14} = g/10^{14} \text{ cm s}^{-2}$, and the subscript ‘b’ signifies that the quantities are taken at the base of the ocean. Note that in Eq. (1) we assume $\langle Z_b^{5/3} \rangle \sim 100$, appropriate

for an oxygen-enriched ocean; a heavy-element rich can be much shallower, $y_b \sim 10^{12} \text{ g cm}^{-2}$.

BC09 showed that when accretion ends, the cooling of the star proceeds by the temperature profile relaxing from the outside-in. At any given time, lower density layers have cooled and adopted a constant flux temperature profile, whereas deeper layers have yet to thermally relax. The transition occurs at a depth given by setting the thermal timescale

$$\tau \simeq \frac{\rho c_P H_P^2}{2K} = 19 \text{ days } y_{14} \left(\frac{T_8}{3} \right)^{-1} \left(\frac{Y_e}{0.4} \right)^2 \left(\frac{g_{14}}{2} \right)^{-1} \quad (2)$$

(Henyey & L’Ecuyer 1969; equation 7 of BC09) equal to the current time. In Eq. (2), ρ is the mass density, c_P is the specific heat, K is the thermal conductivity, and $H_P = -dr/d \ln y = y/\rho$ is the pressure scale height. In the ocean, the pressure is dominated by the relativistic degenerate electrons with $E_F/k_B T = 400 y_{14}^{1/4} (3/T_8)(g_{14}/2)^{1/4}$, giving the scalings $K \propto y^{1/4} T$, $H_P \propto y^{1/4}$, and $c_P \approx 3k_b/Am_p$ and T constant (e.g., MC11 and references therein).

Equations (1) and (2) show that tens of days after the onset of quiescence, the base of the ocean will start to cool and solidify. As new crust is formed, the bottom of the ocean becomes enriched in light elements because of chemical separation (Horowitz et al. 2007; Medin & Cumming 2010). In MC11, we estimated the timescales for particle nucleation, growth, and sedimentation of solid particles, finding that these “microscopic” timescales were much shorter than “macroscopic” timescales such as the time to accrete the ocean, or more relevant here, the time for the ocean to cool. The picture then is that fluid elements with a light composition are deposited at the base of the ocean and will rise upwards, driving convective mixing. Moreover, the convection occurs in a medium that is otherwise thermally stratified. Therefore the convective heat flux, which is proportional to the excess of the temperature gradient $\nabla = d \ln T / d \ln P$ in the star compared to the adiabatic gradient $\nabla_{\text{ad}} \simeq 0.4$, or $F_{\text{conv}} \propto \nabla - \nabla_{\text{ad}}$, is negative; the compositionally driven convection transports heat inwards.

We can estimate the expected size of F_{conv} by comparing the heat and composition fluxes. In mixing length theory, the heat flux is $F_{\text{conv}} \approx \rho v_{\text{conv}} c_P T (\nabla - \nabla_{\text{ad}})$, where v_{conv} is the convective velocity; whereas the composition flux is $F_X \approx \rho v_{\text{conv}} X \nabla_X$, where ∇_X is the composition gradient in the star $\nabla_X = d \ln X / d \ln P$ (MC11), and X is the light element fraction. The convective velocity is given by the superadiabaticity,

$$v_{\text{conv}}^2 \approx gl^2 [\chi_T (\nabla - \nabla_{\text{ad}}) + \chi_X \nabla_X], \quad (3)$$

where l is the mixing length, $\chi_T = \partial \ln P / \partial \ln T|_{\rho, X}$, and $\chi_X = \partial \ln P / \partial \ln X|_{T, \rho}$. In the ocean, the convection is extremely efficient and therefore close to marginal stability, $\chi_T (\nabla_{\text{ad}} - \nabla) \approx \chi_X \nabla_X$. The heat and composition fluxes are then related by

$$F_{\text{conv}} = -c_P T \left(\frac{\chi_X}{\chi_T} \right) \frac{F_X}{X}. \quad (4)$$

During cooling, the composition of the ocean is chang-

ing with time as the ocean is enriched in light elements. For efficient convection, the light element fraction is fairly constant over the ocean ($\nabla_X \approx \chi_T \nabla_{\text{ad}} / \chi_X \propto k_B T / E_F \ll 1$), and so $\partial X / \partial t$ is roughly constant throughout the ocean. The composition flux is then $F_X \approx y (\partial X / \partial t)$, and the heat flux is

$$F_{\text{conv}} = -y c_P T \frac{\chi_X}{\chi_T} \frac{\partial \ln X}{\partial t}. \quad (5)$$

Taking $\chi_X \approx 0.1$ and $\chi_T \approx 10 k_B T / \langle Z \rangle E_F$ (MC11), we find a flux that increases steeply inwards, $F_{\text{conv}} \propto y^{5/4}$.

If cooling is unaffected by compositionally driven convection, we estimate the timescale on which X is changing, $\partial t / \partial \ln X$, to be a typical thermal time at the ocean floor: in the standard cooling model the bulk of the ocean freezes on a thermal time; as it does it releases nearly all of its light elements into the remaining ocean and approximately doubles the light element content there. Equation (5) becomes

$$F_{\text{conv}} \approx -10^{25} \text{ erg cm}^{-2} \text{ s}^{-1} y_{14}^{5/4} \left(\frac{\partial t / \partial \ln X}{10 \text{ days}} \right)^{-1} \quad (6)$$

where we have assumed $Y_e = 0.4$ and $g_{14} = 2$ [and $y_{b,14} = 1$ and $T_8 = 3$ in Eq. (2)]. The flux from compositionally driven convection in Eq. (6) easily outweighs the cooling flux, $\sigma T_{\text{eff}}^4 = 10^{20} \text{ erg cm}^{-2} \text{ s}^{-1} (T_{\text{eff}}/100 \text{ eV})^4$. This suggests that the cooling of an ocean with chemical separation included should be significantly different than without, and motivates our numerical calculations that will be presented in the next section. As we shall see below, the freezing of the ocean is strongly regulated by the convective heat flux, and in turn keeps the heat flux at a much lower level than is suggested by Eq. (6).

3. NUMERICAL SIMULATIONS OF COOLING WITH COMPOSITIONALLY DRIVEN CONVECTION

We solve for the thermal relaxation of the neutron star ocean and crust by solving the thermal diffusion equation following BC09, but including convective heat fluxes modeled using mixing length theory and assuming the convection is efficient as described in MC11, and in addition by following the composition profile as chemical separation and mixing occur. For the examples shown here, we take the ocean composition to be a mixture of oxygen and selenium, for which the phase diagram is shown in the lower panel of figure 1 in MC11. A full description of our numerical code will be presented elsewhere (Medin & Cumming 2013); here we focus on the resulting light curves and describe the influence of compositionally driven convection on the evolution.

Figure 1 shows an example light curve with and without compositionally driven convection included. Figures 2 and 3 show the temperature and composition profiles, respectively, at different times as the ocean and crust cool. We start with a temperature profile at the end of the accretion outburst similar to that assumed by BC09, with an inward directed flux, and $X_b = 0.37$, where X is the mass fraction of oxygen, corresponding to the steady state (MC11). The neutron star mass and radius are $1.62 M_\odot$ and $R = 11.2 \text{ km}$, giving a redshift factor of $1 + z_{\text{surf}} = 1.32$.

We find that the evolution proceeds in four stages. During stage 1, the base of the ocean has not yet started

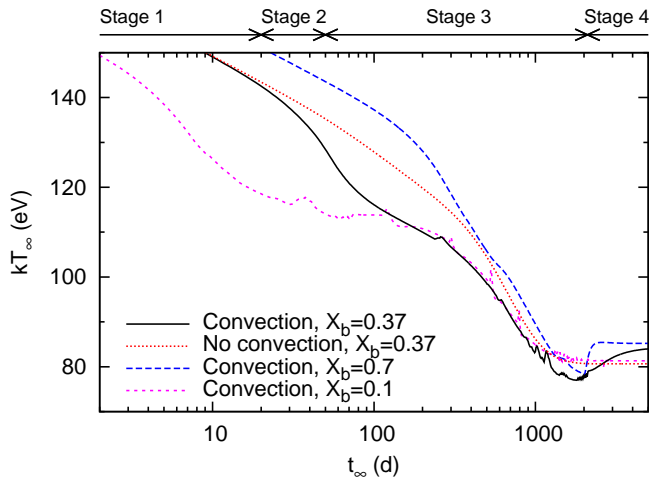


FIG. 1.— Cooling light curves from our numerical simulations, with compositionally driven convection (curves labeled “Convection”) and without (“No convection”). Here, t_∞ is the time from the end of the accretion outburst and T_∞ is the effective temperature (T_{eff}) as seen by an observer at infinity. The curves were generated with the initial temperature profile shown in Fig. 2 and an impurity parameter (cf. BC09) $Q_{\text{imp}} = 0$; the initial base composition X_b for each run is as labeled. The labels that appear above the graph denote the duration of the stages of convection for the “ $X_b = 0.37$ ” case (see text). The spikes and wiggles in the “Convection” curves are the result of the oscillations of ∇_b around ∇_L as described in the text, coupled with our finite numerical resolution.

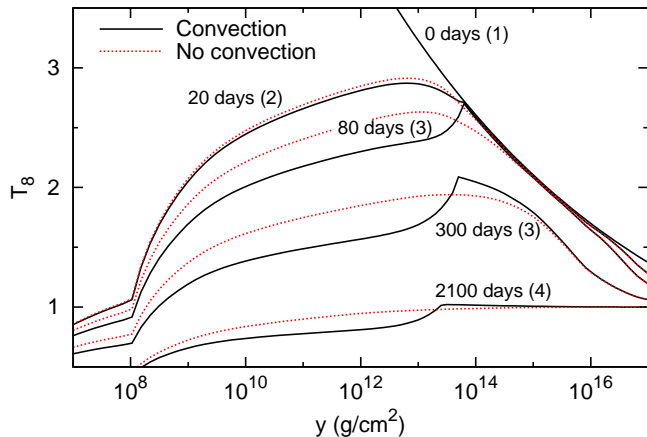


FIG. 2.— Temperature profiles from our numerical simulations during cooling, with compositionally driven convection (solid curves) and without (dotted curves). Each pair of curves is labeled with a t_∞ value and, for the convective models, the stage is given in parentheses. The curves were generated with $Q_{\text{imp}} = 0$ and $X_b = 0.37$ (as in the solid and dotted curves of Fig. 1.)

to cool and so the evolution is the same with or without convection included. The light curve is a power-law with slope given by equation 8 of BC09, with the modification that $\partial \ln \tau / \partial \ln y = 1$ in the ocean rather than $3/4$ as in the outer crust.

In stage 2, the cooling wave has reached the bottom of the ocean, and new crust begins to form, driving convection. Because convection transports heat inward from the ocean to the ocean-crust boundary, cooling at the boundary is delayed at the expense of more rapid cooling in the ocean. As a result, the temperature profile in the ocean becomes very steep (see the 80 days curve in Fig. 2) and the light curve drops faster than without con-

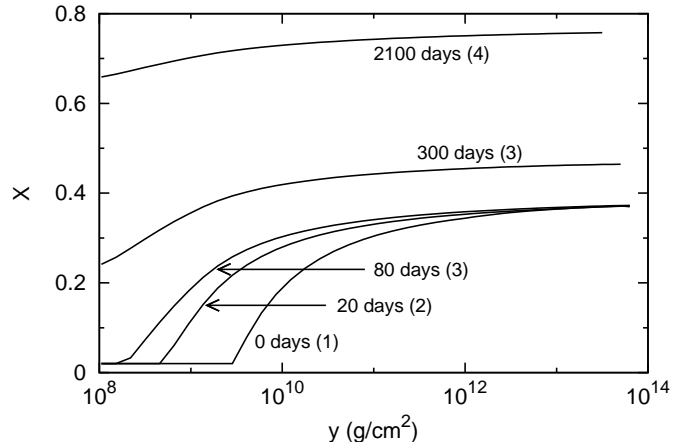


FIG. 3.— Composition profiles from our numerical simulations with compositionally driven convection, at various times during cooling (cf. Fig. 2).

vection (20 days $\lesssim t_\infty \lesssim 80$ days in Fig. 1). During this stage, the convective heat flux is strong and the boundary cools very slowly; the transition depth and temperature y_b and T_b remain close to their values at the onset of quiescence. In this way, the convection acts analogously to the latent heat.¹ The cusp in the temperature profile (Fig. 2) is due to the jump in conductive flux that must occur to balance the large inward convective flux in the ocean.

The temperature profile can not steepen indefinitely, because eventually the temperature gradient at the base of the ocean ∇_b approaches $\nabla_L \simeq 0.25$, the liquidus temperature gradient (i.e., how the melting temperature varies with pressure; see MC11). When $\nabla_b = \nabla_L$, multiple depths at the bottom of the ocean freeze simultaneously. This rapid freezing quickly suppresses itself, however, as strong compositionally driven convection heats the base of the ocean and melts the top of the crust, mixing a heavy-element fluid into the bottom of the ocean and thereby stabilizing the ocean against further convection. Cooling resumes, but convection remains off, such that the steep temperature profile at the ocean base that had been supported by convection quickly flattens due to heat conduction. Once the heavy-element-enriched fluid at the base of the ocean completely solidifies, compositionally driven convection resumes and the temperature profile steepens again.

In this manner ∇_b oscillates around ∇_L . We refer to this phase as stage 3. In this stage convection is sporadic in the ocean and can no longer prevent the ocean base from cooling. As a result, the ocean boundary moves outward and the cooling wave then continues its inward motion through the crust. We find generally that $\partial \ln T_b / \partial t \gg \partial \ln y_b / \partial t$; i.e., that the ocean-crust boundary cools rapidly but moves outward slowly. This is due to the compensating effect of light element enrichment on the freezing depth. During stage 3, the surface temperature T_{eff} still drops with time, but at a rate similar to without convection; and now $\nabla_b = \nabla_L$ is constant while T_b and y_b drop and X_b increases (80 days $\lesssim t_\infty \lesssim 2100$ days in Figs. 1–3).

¹ Note that latent heat is much smaller than the convective heating and does not significantly change the light curve.

During stage 4, the crust is thermally relaxed, the ocean cools too slowly for convection to support the steep gradient $\nabla_b = \nabla_L$, and the light curve returns to the shape it would have if there was no ocean convection ($t_\infty \gtrsim 2100$ days in Figs. 1–3). Note, however, that due to light element enrichment the asymptotic value of T_{eff} is slightly higher in the case with convection than without (the ocean thermal conductivity $K \propto \langle Z \rangle^{-1}$, and so for a given base temperature the outwards flux is greater for a lower $\langle Z \rangle$). Alternatively, the ocean experiences an abrupt transition to stage 4 when the base is saturated with light elements ($X = 1$ for the O–Se example here) and chemical separation halts; this happens at $t_\infty \simeq 2000$ days in the $X_b = 0.7$ case of Fig. 1.

4. DISCUSSION AND CONCLUSIONS

Previous calculations of the thermal relaxation of accreting neutron stars in quiescence have assumed that the ocean cools passively. In contrast, we have shown here that mixing in the ocean driven by chemical separation at the base leads to a significantly different evolution, changing the expected cooling curve. The early time (1–100 days) cooling curve of quiescent neutron stars potentially offers a remarkable new probe of the freezing and chemical separation of a classical plasma in “real time”. The timing of the rapid drop in flux is sensitive to the composition and temperature of the ocean at the end of the outburst. The magnitude of the effect depends on the composition of the ocean, in particular the fraction of light elements and contrast in the atomic mass of the light and heavy nuclei.

The difference in the early-time light curve should also be taken into account when inferring the conditions in the neutron star ocean from observations. For example, BC09 required an additional shallow heat source in their models to reproduce the temperatures seen in the first measurements (at 65 days and 38 days post-outburst respectively) of KS 1731–260 and MXB 1659–29. Including ocean convection will change the derived ocean temperature, we will explore this in a future paper.

Of the four transients with long duration outbursts, perhaps the most interesting source to look at with regard to ocean cooling is XTE J1701–462 (cf. Fig. 4), which is significantly hotter than KS 1731–260 and MXB 1659–29 such that the ocean remains liquid for several hundred days after the outburst. Page & Reddy (2013) were able to fit the light curve with a standard cooling model (neglecting two data points that lie above the underlying trend that are argued to be contaminated with residual accretion). An preliminary fit including convection is shown in Fig. 4.

Recently, observations have been made of two classical transients, showing shorter accretion outbursts of only 2–3 months: the 11 Hz pulsar IGR J17480–2446 in Terzan 5 (Degenaar et al. 2013a), and the transient XTE J1709–267 (Degenaar et al. 2013b). IGR J17480–2446 shows a decaying flux over 2.2 years into quiescence, with the puzzle that the flux remains elevated above the value observed before its 2010 accretion outburst. XTE J1709–267 showed a rapid decrease in temperature during a single 8 hour XMM observation (Degenaar et al. 2013b). If due to crust cooling, Degenaar et al. (2013b) suggested that a strong heat source must be operating at low densities within the ocean during the outburst. A

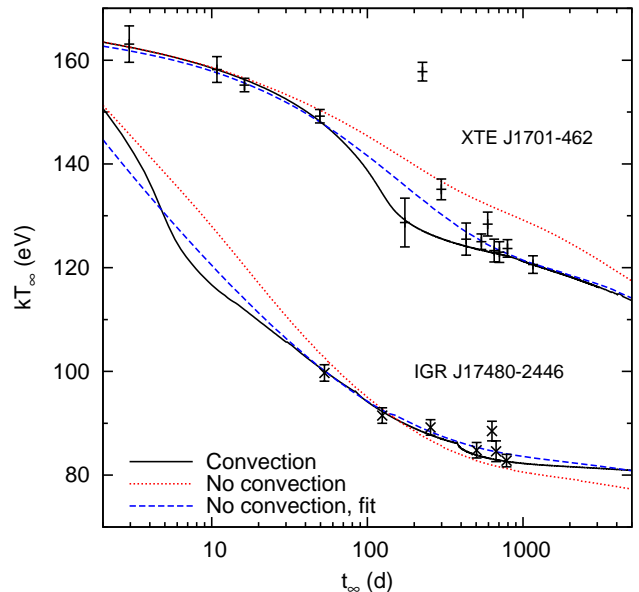


FIG. 4.— Model light curves with compositionally driven convection (solid curves) and without (dashed and dotted curves), plotted over the observations of XTE J1701–462 and IGR J17480–2446 (Fridriksson et al. 2011; Degenaar et al. 2013a). For each source, the solid curve and the dashed curve are intended to fit the observations; while the dotted curve was generated with the same parameters as the solid curve. For XTE J1701–462 we set a hydrogen and helium burning layer at $y_0 = 5 \times 10^7$ g cm $^{-2}$ and a core temperature of $T_c = 1.8 \times 10^8$ K, and use $Q_{\text{imp}} = 40$ and $X_b = 0.37$ for the solid and dotted curves and $Q_{\text{imp}} = 150$ and $X_b = 0.15$ for the dashed curve. For IGR J17480–2446 we set $y_0 = 3 \times 10^9$ g cm $^{-2}$ and $T_c = 8.5 \times 10^7$ K, and use $Q_{\text{imp}} = 100$ and $X_b = 0.15$ for the solid and dotted curves and $Q_{\text{imp}} = 100$ and $X_b = 0.04$ for the dashed curve.

low density heat source is required to achieve a significant thermal relaxation after a short outburst of only 2–3 months. Compositionally driven convection could explain the steep drop observed in XTE J1709–267 as due to rapid ocean cooling — indeed, in our model we can match the observed slope of the light curve with a much smaller heat source when convection is on than when it is off, by choosing the model parameters such that stage 2 of convection (§2) occurs during the observation. Similarly, the general flattening of the light curve due to convection and the higher asymptotic surface flux due to light element enrichment in the ocean could help to explain the prolonged and elevated cooling in IGR J17480–2446 — see Fig. 4.

There remains much to be explored theoretically. We have included only two species in our calculations, oxygen and selenium, which approximates the rp-process ashes used by Horowitz et al. (2007). The phase diagram for multicomponent mixtures is complex but can be calculated (Horowitz et al. 2007; Medin & Cumming 2010) and should be included. We have assumed that solid particles form at a single depth. However, electron capture reactions may occur in the ocean (for example, ^{56}Fe captures at a density of 1.5×10^9 g cm $^{-3}$, Haensel & Zdunik 1990), lowering the $\langle Z \rangle$ at that depth, and potentially leading to formation of solid particles pre-electron capture above the post-electron capture liquid layers. It will be important to include carbon burning in the models. Enrichment of the ocean with carbon remains a major

issue for superburst models (Schatz et al. 2003). Chemical separation during the cooling phase will significantly enrich the ocean in light elements immediately following an outburst, much more efficiently than gravitational sedimentation during quiescence. This may have implications for the puzzling superburst observed immediately before the onset of an accretion outburst in EXO 1745–248 (Altamirano et al. 2012).

We thank Chuck Horowitz, Nathalie Degenaar, and

Chris Fontes for useful discussions. A.C. is supported by an NSERC Discovery Grant and is an associate member of the CIFAR Cosmology and Gravity program. We are grateful for the support of an International Team on Neutron Star Crusts by ISSI in Bern. Z.M. was supported by a LANL Director’s Postdoctoral Fellowship. This research was carried out in part under the auspices of the National Nuclear Security Administration of the U.S. Department of Energy at Los Alamos National Laboratory and supported by Contract No. DE-AC52-06NA25396.

REFERENCES

- Altamirano, D., Keek, L., Cumming, A. et al. 2012, MNRAS, 426, 927
- An, H., Kaspi, V., Archibald, R., & Cumming, A. 2013, ApJ, 763, 82
- An, H., Kaspi, V. M., Tomsick, J. A., et al. 2012, ApJ, 757, 68
- Althaus, L. G., García-Berro, E., Isern, J., Córscico, A. H., & Miller Bertolami, M. M. 2012, A&A, 537, A33
- Bildsten, L. & Brown, E. F. 1997, ApJ, 477, 897
- Bildsten, L., & Cutler, C. 1995, ApJ, 449, 800
- Brown, E. F. & Cumming, A. 2009, ApJ, 698, 1020
- Cackett, E. M., Brown, E. F., Cumming, A., et al. 2013, ApJ, 774, 131
- Cackett, E. M., Brown, E. F., Cumming, A., et al. 2010, ApJ, 722, L137
- Degenaar, N., Wolff, M. T., Ray, P. S., et al. 2011, MNRAS, 412, 1409
- Degenaar, N., Wijnands, R., Brown, E. F., et al. 2013a, ApJ, 775, 48
- Degenaar, N., Wijnands, R., & Miller, J. M. 2013b, ApJ, 767, L31
- Eichler, D., & Cheng, A. F. 1989, ApJ, 336, 360
- Fridriksson, J. K., Homan, J., Wijnands, R., et al. 2011, ApJ, 736, 162
- Haensel, P., & Zdunik, J. L. 1990, A&A, 227, 431
- Hirose, K., Labrosse, S., & Hernlund, J. 2013, Ann. Rev. Earth and Planetary Sciences, 41, 657
- Horowitz, C. J., Berry, D. K., & Brown, E. F. 2007, Phys. Rev. E, 75, 066101
- Medin, Z. & Cumming, A. 2010, Phys. Rev. E, 81, 036107
- Medin, Z. & Cumming, A. 2011, ApJ, 730, 97
- Medin, Z. & Cumming, A. 2013, in preparation
- Page, D. & Reddy, S. 2013, Phys. Rev. Lett., submitted (arXiv:1307.4455)
- Potekhin, A. Y., & Chabrier, G. 2000, Phys. Rev. E, 62, 8554
- Schatz, H., Bildsten, L., Cumming, A., & Ouellette, M. 2003, Nucl. Phys. A, 718, 247
- Shternin, P. S., Yakovlev, D. G., Haensel, P., & Potekhin, A. Y. 2007, MNRAS, 382, L43
- Wilson, H. F., & Militzer, B. 2010, Phys. Rev. Lett., 104, 121101